6. Martian Global Geology

Mars is the fourth planet from the sun and Earth's outer neighbor. Ground–based observations have yielded many albedo features and surface temperatures (mean temperature at solid surfaces ranges between 186 to 268$_\circ$K) similar to those on Earth. One of the earliest observations of Mars was the strong seasonal variation of the polar caps due to an inclination of 25.19°. Both ice caps are similar to those on Earth, but they are also composed of frozen carbon dioxide (CO_2). In summer the northern hemisphere ice cap loses nearly all of its CO_2 ice, exposing an ice cap of water–ice below. It is thought that large quantities of frozen water conceals within the soil and rocks of Mars at mid–to–high latitudes. This idea is strengthened by permafrost patterns in these regions. Despite the thin atmosphere (about 7 mbar surface pressure), mainly CO_2, long–term wind activity is visible in sand dunes (imaged by orbiter missions), and recently in the form of dust devils and clouds.

After a global dust storm abated in 1971, Mariner 9 revealed a hemispherical dichotomy that separates Mars into old, heavily–cratered southern highlands, and younger northern lowlands. The highlands cover about two–thirds of the southern hemisphere and are dominated by numerous impact basins. Imagery from earlier missions such as Mariner 4, 6 and 7 led to the incorrect conclusion that Mars was geologically "dead", like the Earth's moon. A large number of impact basins suggested that these regions of Mars formed during the "heavy bombardment" period, similar to the Moon and the early Earth, which was believed earlier to be caused by impacts of remnant planetesimals from the earliest formation of the solar system. The northern plains cover much of mid and high–latitudes of the northern hemisphere, and show that Mars has had ongoing geological activity, because almost no large craters are visible. The origin of these plains (relatively flat areas) is not fully known. Some regions appear to be covered by lava flows, while others seem to contain lake sediments and features similar to regions on Earth that experienced massive flooding. The cause of this very distinct difference in surface geology between the northern and southern hemispheres remains unclear.

Enormous Martian volcanoes are located near the equator and in vast areas of the northern mid–latitudes. Volcanism is separated into two distinct regions, the Tharsis Rise (including the record–setting Olympus Mons) and the Elysium volcanoes. Volcanism on Mars has been apparently dominated by smoothly flowing lavas similar to those of Hawaii, forming what are known as "shield" volcanoes (due to their low height/area ratio). The close vicinity of some areas also appears to be covered in volcanic ash. Some of these ash deposits appear to be truncated by previously flowing streams, pointing to a much "wetter" past on Mars.

Other indications for liquid water can be seen in stream valleys eroded by precipitation (run–off channels), valleys eroded by the release of huge amounts of water (outflow channels) and so–called chaotic terrain (collapsed ground). The areas of water activity are correlated in space and probably in time with the volcanic units. Due to the large amount of water having run through the channels and the appearance of the northern lowland units, it was suggested that an early Martian ocean may have existed. Morphologies of impact craters and especially ejecta are largely unique to Mars. With their distinctive lobate ejecta deposits, these craters apparently owe their morphology to fluidization of subsurface material, perhaps by melting of ground ice during impact events. The largest known canyon system in the solar system comprising many small interconnected canyons and collectively named the

Valles Marineris, extends southeast from the Tharsis Rise. The canyon system probably developed as a result of crustal stretching ("tectonic extension") and is the main tectonic feature on Mars. Except these tensional fault valleys (grabens) there are no other surface features that suggest that plate tectonics may ever have operated on Mars. Nevertheless, the formation of the northern lowlands is interpreted to relate to plate tectonics (Sleep, 1994).

6.1. What Do Martian Meteorites Tell Us About Mars

Formerly the group of Martian meteorites were named SNCs for the first three meteorites found: **S**hergotty (1865), **N**akhla (1911), and **C**hassigny (1815). The SNC meteorites are petrologically similar, but highly anomalous compared to other meteoritic samples: The young crystallization age of about 1.3 Ga and their classification as igneous achondrites would require a parent body with prolonged igneous activity. Wood and Ashwal (1982) suggested a Martian origin, which was subsequently proven by comparing the isotope composition of gas inclusions and mass spectrometer measurements of the Martian atmosphere at the Viking landing sites (Bogard and Johnson, 1983). Therefore, they are well distinguishable from other differentiated meteorites.

Currently, 31 Martian meteorites are listed at the *Mars Meteorites* – site at JPL (http://www2.jpl.nasa.gov/snc/) and are widely described in the *Mars Meteorite Compendium* (Meyer, 2003). Here, only a subset of 16 samples will be discussed for which composition, radiometric ages, peak shock pressure, and ejection time from Mars are known (see review by Nyquist *et al.*, 2001). These meteorites are classified by their mineralogical composition into groups of basaltic and Lherzolitic Shergottites, Nakhlites (Clinopyroxenites), Chassignites (Dunites), and Orthopyroxenites. Mineralogically all represent basalts and ultramafic cumulates, and evidently are magmatic in origin. They differ not only in their composition but also in crystallization age.

Basaltic Shergottites are considered analogous to terrestrial basalts (McCoy *et al.*, 1992), and possibly reflect different stages of mixing between Martian crust and mantle material. The texture is consistent with those of surface basaltic lava flows. Together with *Lherzolitic Shergottites*, they represent the youngest group of Martian meteorites. Radiogenic Sr–isotopes indicate that these mafic rocks were formed from different magma sources and under different cooling conditions (Borg *et al.*, 1998). *Chassigny* is the only dunite and seems to have fractionally crystallized from a mafic magma body (Floran *et al.*, 1978). Its crystallization history is similar to that of *Nakhlites*. They are clinopyroxenites containing phyllosilicates and secondary evaporite mineral assemblages of Martian origin, thus confirming the presence of liquid water on Mars (Gooding *et al.*, 1991; Bridges and Grady, 2000; Swindle *et al.*, 2000). When compared to terrestrial augite–rich igneous rocks of the Abitibi greenstone belt (Canada), Treiman (1987) concluded that nakhlites formed in shallow intrusions, which are thought to be common in the Tharsis region of Mars. The oldest Martian meteorite is ALH 84001, a coarse-grained brecciated *Orthopyroxenite*, in which younger carbonates are present. This small amount of carbonates (1%) drew worldwide attention when McKay *et al.* (1996) argued for polycyclic aromatic hydrocarbons (PAH), oxide and sulfide biominerals, and nanofossil-like structures suggesting fossil life on Mars.

Meanwhile, numerous non–biogenic formation mechanisms have been proposed: The PAHs could be due to terrestrial contamination (Becker *et al.*, 1997; Jull *et al.*, 1998), and carbonates and magnetite assemblages might be flood evaporites (McSween and Harvey, 1998; Warren, 1998).

The radiometric crystallization ages of these different Martian meteorite classes indicate the

Martian Meteorite Summary

Meteorite	Age° in Ma	Ejection Age* in Ma	Shock pressure+ in GPa
Shergottites (Basalts):			
Shergotty	165 ± 4	2.73 ± 0.15	29 ± 1
Zagami	177 ± 3	2.92 ± 0.20	31 ± 2
Los Angeles	170 ± 8	3.10 ± 0.20	∼ 35–40
EETA79001A	173 ± 3	0.73 ± 0.15	34 ± 2
EETA79001B	paired (EETA79001A)		
QUE 94201	327 ± 10	2.71 ± 0.20	∼ 30–35
DaG 476	474 ± 11	1.24 ± 0.12	∼ 35–40
Dhofar 019		19.8 ± 2.3	∼ 35–40
SaU 005		1.5 ± 0.3	∼ 35–40
Shergottites (Lherzolites):			
AHLA77005	179 ± 5	3.06 ± 0.20	43 ± 2
LEW88516	178 ± 8	3.94 ± 0.40	∼ 45
Y793605	212 ± 62	4.70 ± 0.50	∼ 45
Clinopyroxenites (Nakhlites):			
Nakhla	1270 ± 10	10.75 ± 0.40	∼20 (±5)
Governador	1330 ± 10	10.0 ± 2.1	∼20 (±5)
Valadares	paired (Governdor)		
Lafayette	1320 ± 20	11.9 ± 2.2	∼20 (±5)
Dunite:			
Chassigny	1340 ± 50	11.3 ± 0.6	∼ 35
Orthopyroxenite:			
ALH 84001		15.0 ± 0.8	∼ 35–40
Silicates	4510 ± 110		
Carbonates	3920 ± 40		

°The preferred crystallization age is given (see Nyquist *et al.*, 2001).
*Mars ejection age calculated as the preferred cosmic–ray exposer age and terrestrial residence time (see Nyquist *et al.*, 2001).
+Estimated peak shock pressure after Stöffler and Weber (1986) Stöffler (2000); Nyquist *et al.* (2001).

Table 6.1.: Martian Metorites: Summary of radiometric crystallization ages, estimates of the peak shock pressure induced during the ejection process, and time since the ejection from Martian surface separated by compositional group.

existence of surface or near–surface rocks (i.e. volcanism) on Mars with ages of about 175 Ma, 300 – 500 Ma, 1.3 Ga and 4.5 Ga, which cover an age spanning the entire history of Mars. Together with their composition, this suggests magmatic activity from planet formation until recent times. The young ages agree with ages derived from crater counts for volcanic provinces in Tharsis, Elysium and Amazonis region (cf. Chapter 15.5). The samples, which contain evaporitic phases, possibly indicate the presence of liquid water at around 3.9 Ga and

even 1.3 Ga ago, i.e. the period in which landforms related to fluvial activity are found (cf. Chapter 14.6).

The widely accepted idea of delivering rocks from planet–to–planet is ejection from the planet's surface by large scale impacts. For Mars, the ejection velocity is about 5 km/s. All Martian meteorites are moderately to strongly shock–metamorphosed by peak shock pressures of between 15 and 45 GPa. Rocks which have left the Martian surface have not been molten, but it is likely that the shock metamorphism is related to the ejection event and possibly a function of parent body size (Table 6.1). In this respect, the recent ejection age (less than 20 Ma) and the fact that all samples are of magmatic/volcanic origin is interesting. Ejection and transport mechanism will be discussed later in respect with secondary cratering in a later chapter.

The most reliable crystallization ages of the meteorites span from the formation of the planet nearly to present, while only a single Martian rock is older than 1.3 Ga. This is a rather incomplete set of Martian surface ages and no provenance can be clearly assigned, but they are the only samples from Mars, and of vital importance in understanding its formation and evolution. Nevertheless, radiometric ages provide absolute calibration marks (in terms of setting a time–frame) for relative crater counting records, support absolute ages derived from crater counts through cratering chronology models, and will be discussed in later chapters.

6.2. The Viking–based Stratigraphic System of Mars

A stratigraphic overview of Mars is commonly given by the major physiographic provinces and assemblages as they are shown in a set of 1:15 M–scale maps (Figures 6.1, 6.2, by Scott and Tanaka (1986); Greeley and Guest (1987); Tanaka and Scott (1987)). These maps reflect the overall relation of rock units, their areal distribution, the processes by which they are formed and modified, and the recorded geologic history. The Martian stratigraphic system is based on the identification and delineation of geologic units. They are identified according to their topography, morphology, and spectral properties as recorded from spacecraft images. Relative ages are determined by superposition and intersection of the units and globally by the concentration of impact craters superimposed on the geologic unit, thus providing the local history of regions as well as the geological evolution of the entire planet. This procedure has been applied by Soderblom *et al.* (1974) and is discussed in detail by Condit (1978) for Mars. Historically, the Mariner 9 mission was the first to give a global view of the Martian surface. The dichotomy, dividing Mars into densely cratered southern highlands and smoother northern lowland plains, was confirmed (Scott, 1978). The impression of Mars being moon–like (Mariner 4) rather than Earth–like was revised. Tectonic, volcanic, eolian, and degradational terrains were revealed so that a global geologic time scale could be established: The Amazonian, Hesperian, and Noachian Epochs (Scott and Condit, 1977). Based on high resolution Viking Orbiter imagery, more detailed stratigraphic investigations were undertaken, and more geologic classes as well as a subdivision of the stratigraphy were introduced.

The current time-stratigraphic system of chronologic periods and epochs to subdivide the Martian geologic history was established by Tanaka (1986) and later summarized by Tanaka *et al.* (1992a).

The major geologic division has been mapped and is fundamentally based on the dichotomy: (A) Highland rocks, including the impact basins (Hellas, Argyre, and Isidis) and the southern highland plains; (B) Lowland rocks, the northern plains assemblage, and degraded, ancient rocks along the highland lowland boundary; (C)

Martian Epochs

Epochs	Crater–Frequency Range		
	N(2)⋆	N(5)⋆	N(16)⋆
Upper Amazonian	< 40		
Middle Amazonian	40–150	< 25	
Lower Amazonian	150–400	25–67	
Upper Hesperian	400–750	67–125	
Lower Hesperian	750–1200	125–200	< 25
Upper Noachian		200–400	25–100
Middle Noachian		> 400	100–200
Lower Noachian			> 200

⋆ N(D) = cum. number of craters with diameters ≥D, normalized to an area of 10^6 km^2

Table 6.2.: The crater frequencies for crater diameters equal to or larger than 2 km, 5 km, and 16 km, which outline the boundary conditions for the different geological epochs from Tanaka *et al.* (1992a).

Volcanic and tectonic regions, including highland paterae, the Tharsis and Elysium volcanic regions and Valles Marineris; (D) Channel systems, mostly emanating from chaotic terrains close to Valles Marineris; (E) Polar regions, including mantling, polar layered and ice deposits. Geologic type regions have been assigned to the three major time–stratigraphic systems: The oldest Noachian System is named after the ancient cratered and rugged terrain in Noachis Terra (Scott and Carr, 1978). The overlying Hesperian System got its name from ridged plains material represented in Hesperia Planum. The boundary to the most recent Amazonian System has been defined based on the Arcadia Formation in the Amazonis quadrangle, consisting of smooth plains material. This scheme follows developments of terrestrial geology based on the fundamental principle of classifying rocks according to their relative ages (James Hutton and William Smith), long before absolute ages emerged at around 1910. Tanaka's subdivision scheme is based on cumulative crater counts, carried out at different crater diameter ranges in the type areas defining the stratigraphic base of these periods and epochs (e.g. older units are defined by larger craters whereas younger units are defined by smaller craters). The boundaries based on these crater counts are given in Table 6.2. Therefore, he assumed a "minus–two" power–law for the crater diameter distribution. Their cumulative frequencies, base of these periods and epochs, have been recalculated to cumulative frequencies for 1-km craters, and absolute ages were determined from the new unified Martian chronology model by Hartmann and Neukum (2001) (compare Fig. 5.1). All absolute ages given in this thesis are calculated on the basis of equation 11.2, and the Martian crater production function following Neukum (1983) and its updated expression by Ivanov (2001), if not stated otherwise. Any stratigraphic classification is based on the re–measured time–stratigraphic units (Fig. 5.1). Data from the Mars Global Surveyor (MGS) spacecraft has already provided new insights into Martian stratigraphic relationships and the timing of major geological events. Due to the high–resolution imagery, specific stratigraphic issues regarding timing, and extent of resurfacing activity (volcanic and fluvial) have been raised.

Several first–order refinements to improve the Viking-based scheme have been achieved:

1. Tanaka's original crater size–frequency distributions were recalculated to a 1-km cumulative crater frequency using the new Mars production function polynomial by Ivanov (2001).

2. The corresponding cratering model age was calculated for each type area, using equation 11.2.

3. Counts on new images returned from the Mars Global Surveyor Camera redefined the Lower Amazonian base corresponding to a slightly younger cratering model age of 3.14 Ga (Hartmann and Neukum, 2001), revealed by the smaller crater size range not seen in Viking imagery.

Major geological events in Mars history, derived from stratigraphic analysis of geologic units and corresponding crater densities, grouped by geological processes (Head *et al.*, 2001) are in Fig. 6.3.

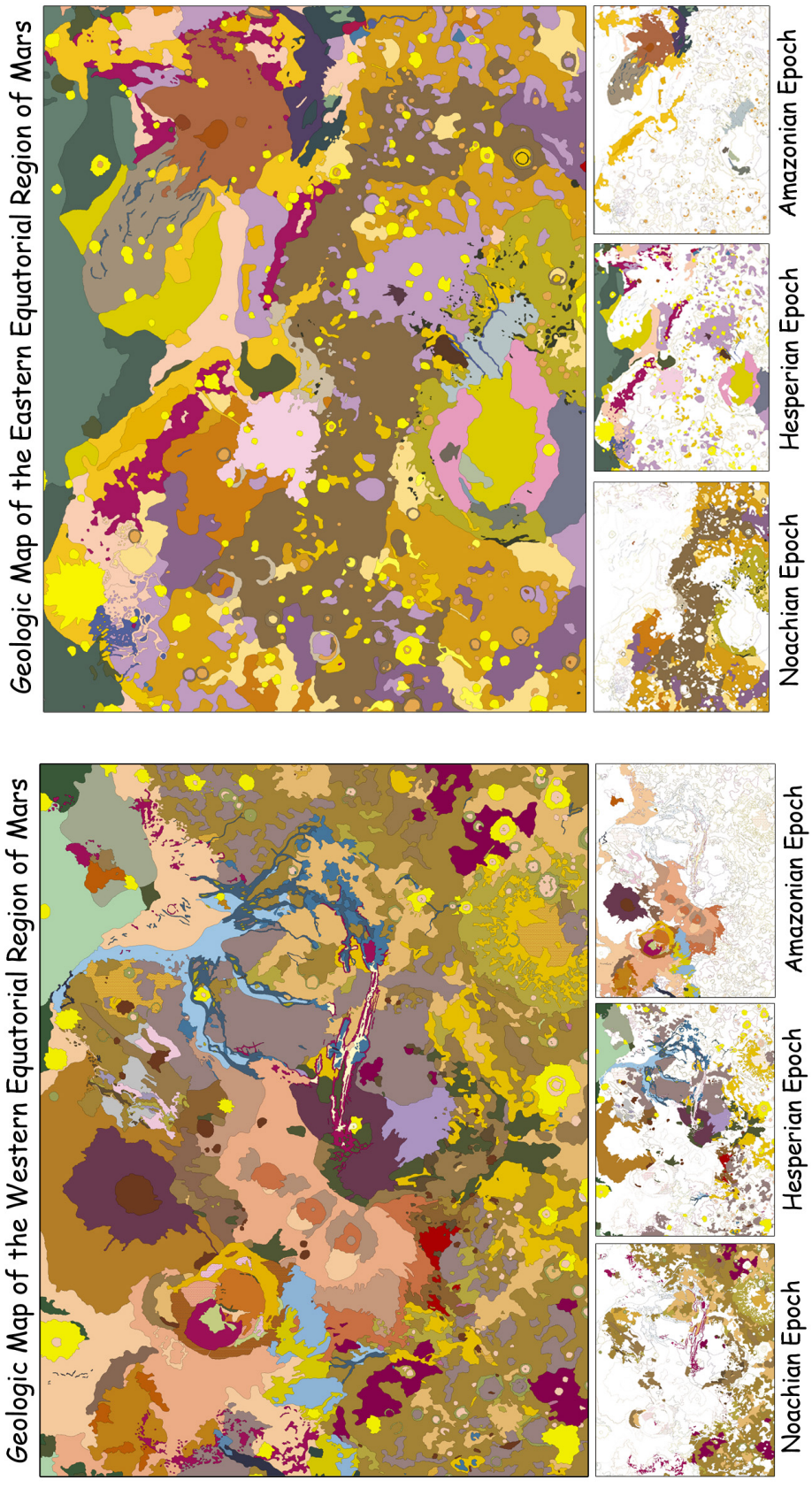

Figure 6.1.: Geologic map of the Western (left) and Eastern (right) region of Mars, from Scott and Tanaka (1986); Greeley and Guest (1987). In the small sketches units are highlighted according to the Noachian, Hesperian and Amazonian time units.

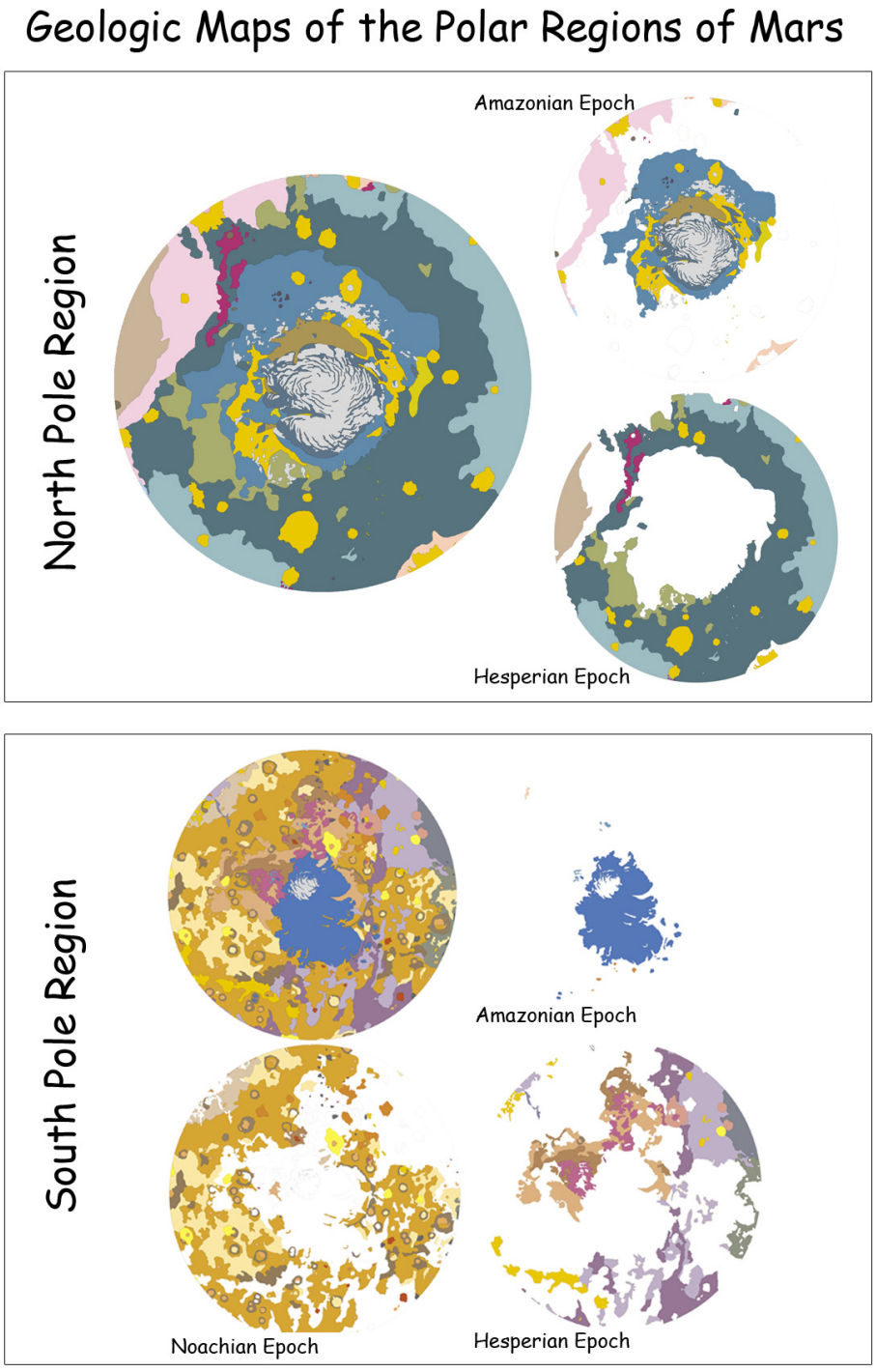

Figure 6.2.: Geologic map of the polar regions of Mars, from Tanaka and Scott (1987). The North–pole region is shown in the upper part (no Noachian units). Below, the South–pole region is shown with sketches highlighting the Noachian, Hesperian and Amazonian time units.

6.3. Towards A New Time–Stratigraphy

As stated already in Chapter 3, various stratigraphic units have been mapped on Mars and their relative ages have been determined from a combination of superposition relations and crater frequencies (Neukum and Hiller, 1981; Tanaka, 1986; Scott and Tanaka, 1986; Greeley and Guest, 1987; Tanaka and Scott, 1987). In principle, absolute ages can be estimated through impact crater frequencies. The absolute chronology and absolute ages of different Martian stratigraphic units had been known only crudely due to uncertainties in the Martian impactor flux. One approach to extract the cratering production function from the geologically distorted record is to transfer the well–known and measured production function of the Moon to Mars by considering impact rate, scaling laws and possible influence of target properties (Neukum and Wise, 1976). The problem with this method is a gap in the image resolution that is demonstrated in Section 12. Older models for understanding the flux in Martian surroundings (Chapter 3) had produced, based on Viking and Mariner 9 data analysis, a wide range of chronologic systems with no clear consensus on the absolute ages (Hartmann, 1973; Soderblom *et al.*, 1974; Neukum and Wise, 1976; Hartmann *et al.*, 1981; Neukum and Hiller, 1981; Neukum, 1983; Strom *et al.*, 1992). A variety of observations initiated debates which processes are responsible. The lack of smaller craters (250 m $<$ D $<$ 16 km) in heavily cratered terrain where the largest craters (D $>$ 64 km) had crater densities similar to those in the lunar highlands (that indicate ages of 3.8 to 4.5 Ga (Leighton *et al.*, 1965)) suggested loss of smaller craters by erosion and deposition (Öpik, 1965, 1966). The variety of observations initiated debates which processes are responsible. As mentioned before (Chapter 3) steady rates of obliteration are not applicable, changes in atmosphere thickness (Sagan *et al.*, 1973; Pollack *et al.*, 1987), increased volcanism (Greeley and Spudis, 1981), the abundance of permafrost associated with creep deformation (Squyres and Carr, 1986) and/or sporadic glacial erosion are plausible explanations. Youngest volcanic units imaged by Mars Global Surveyor at image resolutions of up to 1.5 m/pixel launched further debates. Crater statistics for restricted areas, e.g. Elysium Planitia, indicate ages less than 100 Myr or even 10 Myr (Hartmann and Berman, 2000). Furthermore, massive layering and mobility of dust and fine material is confirmed by Malin (1998) from MGS images.

The current understanding of the geologic history of Mars is mainly based on crater size–frequency measurements carried out on high resolution Viking imagery. Several chronology models were published by different investigators (e.g. Soderblom *et al.*, 1974; Neukum and Wise, 1976; Neukum and Hiller, 1981; Hartmann *et al.*, 1981). The most up–to–date reviews of the Martian impact cratering chronology are found in Hartmann and Neukum (2001) and Ivanov (2001). Until recently, it was not possible to measure the Martian crater size–frequency distribution over the full crater–diameter size range due to a resolution gap in the imagery database. Only with the imagery of the High Resolution Stereo Camera onboard Mars Express, a multiple line scanner instrument, has been acquiring high–resolution color and stereo images of the Martian surface (Neukum *et al.*, 2004), and is it now possible to fill this gap. High resolution up to 10 meters per pixel coupled with a large areal extent (swaths typically 60-100 km wide and thousands of km long) means that small details can be placed in a much broader context than was previously possible. Based on the comparison between crater counts over the entire crater diameter size range, the analytically transfered crater size–frequency distribution can be verified.

Mars: Major events in geological history

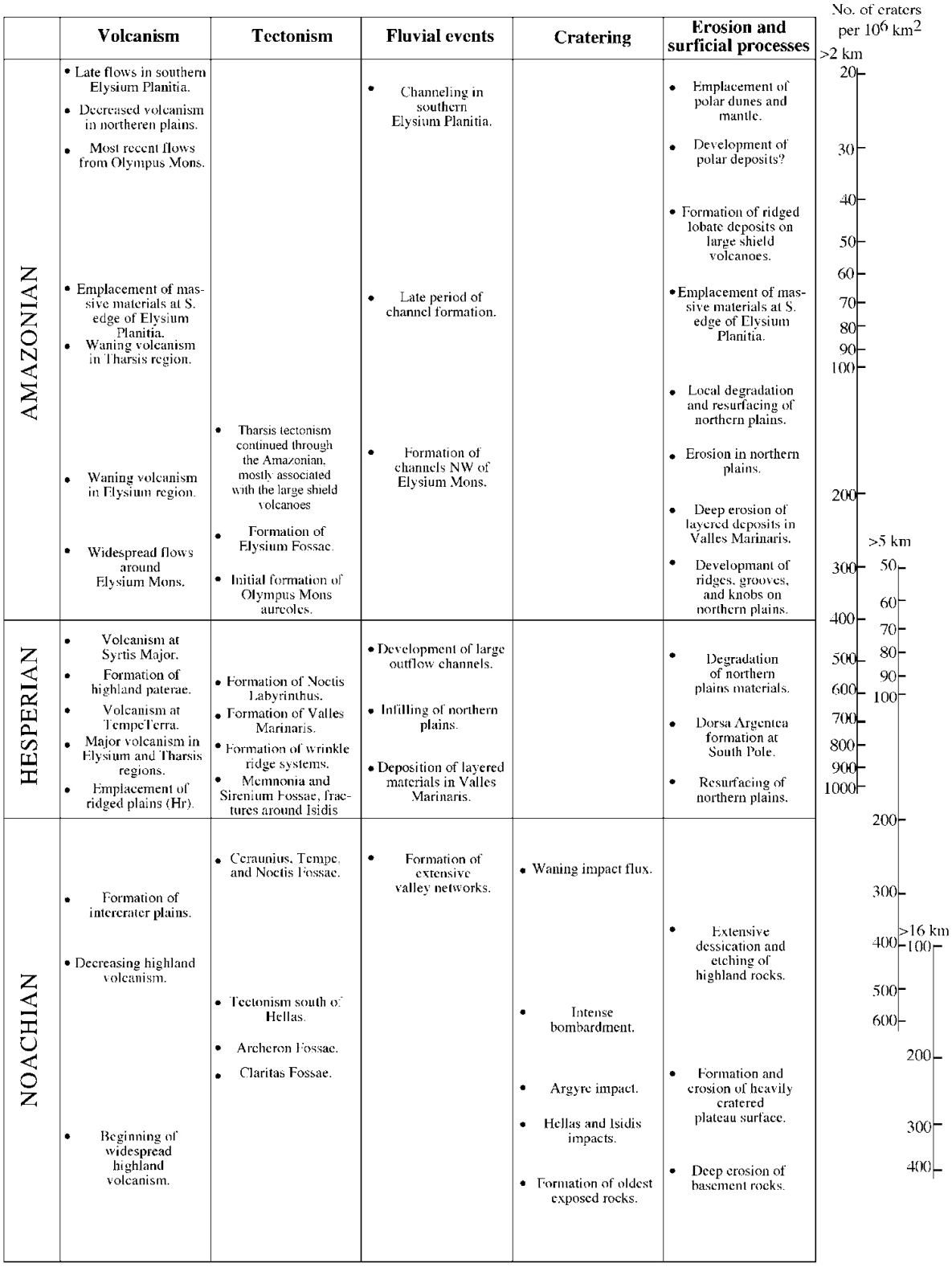

	Volcanism	Tectonism	Fluvial events	Cratering	Erosion and surficial processes
AMAZONIAN	• Late flows in southern Elysium Planitia. • Decreased volcanism in northeren plains. • Most recent flows from Olympus Mons. • Emplacement of massive materials at S. edge of Elysium Planitia. • Waning volcanism in Tharsis region. • Waning volcanism in Elysium region. • Widespread flows around Elysium Mons.	• Tharsis tectonism continued through the Amazonian, mostly associated with the large shield volcanoes • Formation of Elysium Fossae. • Initial formation of Olympus Mons aureoles.	• Channeling in southern Elysium Planitia. • Late period of channel formation. • Formation of channels NW of Elysium Mons.		• Emplacement of polar dunes and mantle. • Development of polar deposits? • Formation of ridged lobate deposits on large shield volcanoes. • Emplacement of massive materials at S. edge of Elysium Planitia. • Local degradation and resurfacing of northern plains. • Erosion in northern plains. • Deep erosion of layered deposits in Valles Marinaris. • Developmant of ridges, grooves, and knobs on northern plains.
HESPERIAN	• Volcanism at Syrtis Major. • Formation of highland paterae. • Volcanism at TempeTerra. • Major volcanism in Elysium and Tharsis regions. • Emplacement of ridged plains (Hr).	• Formation of Noctis Labyrinthus. • Formation of Valles Marinaris. • Formation of wrinkle ridge systems. • Memnonia and Sirenium Fossae, fractures around Isidis	• Development of large outflow channels. • Infilling of northern plains. • Deposition of layered materials in Valles Marinaris.		• Degradation of northern plains materials. • Dorsa Argentea formation at South Pole. • Resurfacing of northern plains.
NOACHIAN	• Formation of intercrater plains. • Decreasing highland volcanism. • Beginning of widespread highland volcanism.	• Ceraunius, Tempe, and Noctis Fossae. • Tectonism south of Hellas. • Archeron Fossae. • Claritas Fossae.	• Formation of extensive valley networks.	• Waning impact flux. • Intense bombardment. • Argyre impact. • Hellas and Isidis impacts. • Formation of oldest exposed rocks.	• Extensive dessication and etching of highland rocks. • Formation and erosion of heavily cratered plateau surface. • Deep erosion of basement rocks.

Figure 6.3.: Tabulated description of the major events in the martian geological history, sorted by geological processes including volcanism, tectonism, fluvial action, cratering, as well as erosion and surficial deposition, from Head *et al.* (2001). On the right–hand side, the relative surface ages, expressed as number of craters greater than the indicated diameter per 10^6 km^2 of surface area, are given (cf. Table 6.2 from Tanaka (1986).

6.4. The Geophysical Mars after Mars Global Surveyor

The Mars Global Surveyor (MGS) mission not only allowed access to a detailed topography through the laser measurements, but also mapped the gravity field through two–way Doppler tracking of the spacecraft (Smith *et al.*, 1999a,b). Based on the topography (Fig. 6.4, A) and the gravity fields a map of the of the present crustal distribution was derived (Fig. 6.4, B) (Zuber *et al.*, 2000; Neumann *et al.*, 2004). Both the topography and the crustal thickness confirmed the dichotomy between the smooth northern lowlands and the cratered southern highlands. The latter is defined by higher elevation and thicker crust, but especially in the vicinity of Arabia Terra, the boundary deviates between the morphologically defined and the separation due to crustal thickness. Neumann *et al.* (2004) arrived with average crustal thickness values for beneath the northern lowlands and southern highlands of about 35 and 60 km, respectively. As a result of such a detailed topography, numerous partially buried impact craters and basins have been identified in the lowland regions and led to the idea that the crust of the lowlands and highlands, similarly densely cratered originally, formed both by the Early Noachian (Frey *et al.*, 2002). The crustal dichotomy could be explained by long–wavelength mantle convection (Nimmo and Tanaka, 2005), very early in the Martian history. Subsequently, this crustal distribution was obscured by the formation of the large impact basins, Hellas, Argyre, Isidis and Utopia.

The detection of different compositions of the northern and southern hemisphere by the Thermal Emission Spectrometer suggests two crustal rock types (Bandfield *et al.*, 2000). One of more basaltic composition (like the composition of Martian meteorites) is confined for the older surface, and one more silica rich (andesitic) component in the lowlands. Wänke *et al.* (2001) interpreted the in situ analysis of Martian rocks by the Pathfinder mission to be of two major chemical components, which confirms the remote sensing detection, but also imply a differentiation history and yield constraints for dynamical models (see Spohn *et al.* (2001) or Solomon *et al.* (2005)). Despite the detection of more andesitic composition in the younger northern lowlands, an andesitic composition is assumed for the ancient crust, and a basaltic composition for later volcanic products (Nimmo and Tanaka, 2005).

Doppler and range measurements to the Mars Pathfinder lander gave further insight into the precession rate of the rotational axis (Folkner *et al.*, 1997) and therefore information on the distribution of mass within the planet. The derived moment-of-inertia (e.g. Sohl *et al.*, 2005) implies that Mars possesses a dense metallic core. While plate tectonics cools the mantle and supports driving an early dynamo (Nimmo and Stevenson, 2000), an initially hot core also sufficiently explains an early dynamo without plate tectonics and allows to consistently explain the Martian thermal evolution better (Breuer and Spohn, 2003).

The detection of remnant magnetization dominantly in the southern hemisphere (Fig. 6.4, C), implies an ancient global self–sustained dipole magnetic field (Acuña *et al.*, 1999), which requires a partly fluid metallic core. The global distribution of magnetic anomalies, their presence or lacking correlated to Martian morphology (northern lowlands, volcanic constructs, and large impact basins in the southern highlands), suggests that parts of the crust formed or were erased by different processes (shock, heating, redistribution), after the core dynamo had ceased (Acuña *et al.*, 1999). Models and observations suggest that the cessation of the dynamo, including the loss of core heat, occurred already very early in Martian history (e.g. Stevenson, 2001).

The identification of young lava flows in the Arsia Mons caldera (about 100 Ma), were found by crater counts on Mars Orbiter Camera images (Hartmann, 1999a). It suggests that Mars has been volcanically active until very recently. The age is supported by crystallization ages

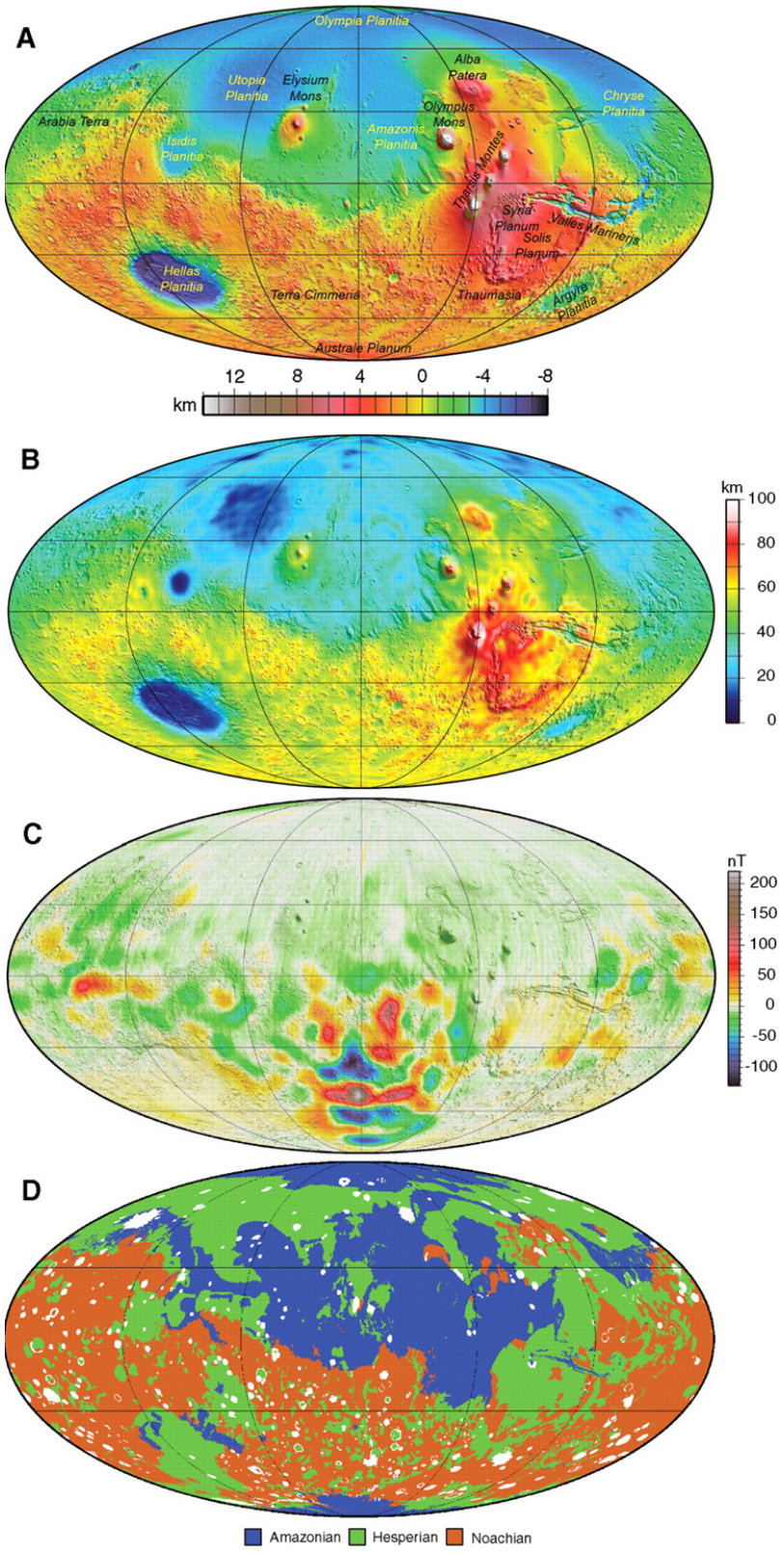

Figure 6.4.: (A) Topographic map of Mars (Smith *et al.*, 1999a; Neumann *et al.*, 2004) with major regions noted. (B) Crustal thickness on Mars (Neumann *et al.*, 2004) for a density contrast at the crust-mantle boundary of 600 kg/m3. (C) Radial component of the magnetic field arising from crustal magnetic anomalies on Mars (Connerney *et al.*, 1999) at an altitude of 400 T 30 km. (D) Map of martian surface units grouped on the basis of age (Scott and Tanaka, 1986; Greeley and Guest, 1987; Tanaka and Scott, 1987). Units transitional between Noachian and Hesperian and between Hesperian and Amazonian have been included in the younger of the two epochs. Areas in white are impact craters and their ejecta deposits. All maps are in Mollweide projection, with 180–longitude at the central meridian (Fig. from Solomon *et al.*, 2005).

of Martian meteorites (see Section 6.1). Considering the formation of Tharsis as one focal point of Martian volcanism that occurred after the global dichotomy had formed, global mantle convection models have to account for long–lived sources in this region (e.g. Stevenson, 2001; Spohn *et al.*, 2001).